Biomedical Microdevices _####################_
https://doi.org/10.1007/s10544-021-00576-x

Fabrication of novel-shaped microneedles to overcome the disadvantages of solid microneedles for the transdermal delivery of insulin

Yuki Mizuno[1] · Kanae Takasawa[1] · Taichi Hanada[1] · Kyou Nakamura[1] · Kazuya Yamada[1] · Hirotada Tsubaki[1] · Masaya Hara[2] · Yasunori Tashiro[2] · Masaaki Matsuo[2] · Takahiro Ito[1] · Tomohiro Hikima[1]

Accepted: 12 July 2021

Abstract

In this study, we fabricated two different microneedles (MNs) — semi-hollow and bird-bill — to overcome the limitations of solid and coated MNs, respectively. The two MN arrays were developed using a general injection molding process to obtain high-quality MNs with uniform shape. The semi-hollow and bird-bill MNs could penetrate the micropores of swine skin up to depths of 178.5 ± 27.6 μm and 232.1 ± 51.3 μm, respectively. When the semi-hollow MNs were used for the transdermal delivery of insulin in diabetic rats, it was observed that the blood glucose concentration (BGC) decreased remarkably within 30 min, and the desired effect of insulin was maintained for an additional 3 h after the removal of insulin from the skin surface. The bird-bill MN was able to load a coating gel at a maximum capacity of 3.20 ± 0.21 mg per MN array, and the BGC continued to decrease significantly after MN application for up to 2–6 h. In summary, we fabricated semi-hollow and bird-bill MN arrays using the injection molding method; these can be mass produced and are capable of effectively producing micro-holes in the stratum corneum. The two MN arrays could provide effective transdermal delivery of large-molecular-weight drugs such as insulin.

Keywords Transdermal drug delivery · Solid microneedle · Injection mold · Biocompatibility · Diabetic rat

Abbreviations

MN	Microneedle
SC	Stratum corneum
TEWL	Trans-epidermal water loss
MEMS	Micro-electro-mechanical system
STZ	Streptozotocin
OCT	Optical coherent tomography
BGC	Blood glucose concentration

1 Introduction

Microneedle (MN) arrays consist of fine needles measuring several hundred micrometers (μm), and they have been used to overcome some of the disadvantages associated with conventional hypodermic or intravenous injections. Based on design and usage, MNs can be classified into four types as follows: hollow MNs, dissolving MNs, solid MNs, and coated MNs. It is important to consider the geometries (Römgens et al. 2014; Kim et al. 2018; Lahiji et al. 2019) and penetration force (Cheung et al. 2014) of MNs in the context of effective transdermal administration of drugs. Mechanical stability of MNs is also essential for achieving reliable skin penetration. Kim et al. (2018) showed that obelisk-type microneedles possess better mechanical stiffness than pyramidal microneedles. A solid, cone- or pyramid-like MN easily opens the micropores on the surface of the skin's stratum corneum (SC) (Larrañeta et al. 2016).

There are several advantages to MNs: skin penetration enhancement occurs via a clear and persuasive mechanism; hydrophilic drugs with high-molecular-weight independent of physicochemical properties are absorbed through the skin; can be used for self-administration; and special equipment such as a power source is not required. However, one disadvantage is that owing to the wound healing ability of the skin, the holes made by MNs are closed over time with the aid of residual SC cells in the area (unpublished data); therefore, the resulting clinical

✉ Tomohiro Hikima
hikima@bio.kyutech.ac.jp

[1] Kyushu Institute of Technology, 680-4 Kawazu, Iizuka, Fukuoka 820-8502, Japan

[2] Mishima Kosan Co., Ltd, 2-1-15 Edamitsu, Yahatahigashi, Kitakyushu 805-0002, Japan

effect caused by the poke and patch MN may decrease over time. Concerns have been raised regarding the limited doses of coated drugs on the surface of the coated MNs (Jin et al. 2018). Hence, various shapes of coated MNs have been designed in order to increase the mass of the coated drug. Gill et al. (2008) reported that MN arrays containing 1,000 needles within a pocket could deliver 100 μg of drug into the skin. Bio-inspired, tear-drop structures on pyramidal MNs increased the liquid coating fluorescence intensity as high as 15 times of that seen using the non-structured MN (Plamadeala et al. 2020). In addition, the shape of the coated MN must be designed to deliver the coated drug and overcome the insertion forces into the skin.

Han et al. (2009) fabricated a complex-shaped MN to create sustainable micropores. As the shape of a MN array is influenced by the microfabrication method used, only simple solid MNs have been put into practical use. Micro-electro-mechanical system (MEMS) technology has been used for manufacturing the desired MN structure (Ribet et al. 2018; Ruggiero et al. 2018). However, MEMS is a relatively expensive technology, considering the complicated processes involved and the requirement of several steps to fabricate high-quality MNs. In contrast, although 3D printing technology can help in developing a complex shape (Johnson et al. 2016; Economidou et al. 2019), it is not suitable for mass production of MNs. Injection molding is a technique in which a polymer is heated and kneaded in a heating cylinder to reach the fluidized state. The fluidized polymer is then pressurized and injected into the cavity of a metal casting mold, and finally cooled and solidified. Although this automated method can support mass production, the MNs thereby produced have, to date, been limited to those of a conical shape.

Therefore, in this study, we proposed new shapes for MNs for efficient drug delivery through the SC. In addition, we also developed a process for the inexpensive mass production of MNs of these shapes using injection molding technology. The semi-hollow MN and bird-bill MN were designed to be used to replace solid and coated MNs, respectively. The effectiveness of the two MN designs was investigated using transdermal administration of insulin, a large-molecular-weight drug, in diabetic rats.

2 Materials and methods

2.1 Materials

A biocompatible polymer, polycarbonate (PC; NOVAREX®, medical grade), was purchased from Mitsubishi Engineering-Plastic Co. (Tokyo, Japan). Metolose® (a derivative of hydroxypropyl methylcellulose; 60SH and TC-5E, medical grade) was acquired from Shin-Etsu Chemical. (Tokyo, Japan). Insulin (from bovine pancreas) was obtained from Sigma-Aldrich Co. (Tokyo, Japan). Methylene blue trihydrate (MB), streptozotocin (STZ), and other reagents were purchased from Fujifilm Wako Pure Chemical Co. (Osaka, Japan).

2.2 Design of MNs

We designed the two MN's shapes to overcome and improve the disadvantages of the solid and coated MN. The MN arrays were designed to contain 100 needles in a circle with an area of 0.44 cm^2. The semi-hollow MN had a punch blade-shaped needle tip, which made the micro-holes on the SC for the poke and patch MN. A cross section of the semi-hollow MN is shown in Fig. 1a. The holes were expected to be maintained on the SC after the skin penetration, thereby enhancing the effects of the MN for a long-term. The bird-bill MN, used to replace the coated MN, had a vertical groove in its tip, which was designed to increase the amount of coated drugs in its groove using capillary attraction (Fig. 1b). The shape of the conventionally coated MN was similar to a barrel when the drug was coated on the MN surface, and almost all of the drug on the needle was retained and wasted on the skin surface upon skin insertion. The drug in a vertical groove of the bird-bill MN was firmly inserted into the skin.

2.3 Micromachining of the MN arrays

The molds for this study were prepared from aluminum. Although, it is not a commonly used material for this purpose, it is easy to cut and pierce at the micro-scale, as required in this study. The MN array molds were fabricated by machining, specifically end milling. The injection molding machine used in this study was ROBOSHOT S-2000i 100B (FANUC Co. Yamanashi, Japan). We used PC as the polymer owing to its advantages of biocompatibility and mechanical strength.

To evaluate the MN arrays, a digital microscope camera was used to capture images (PXHD30UTH, Primetech Engineering Co., Tokyo, Japan; and DSX510, Olympus Co., Tokyo, Japan). The heights and diameters of the MNs were measured using a shape laser microscope (VK-9710, Keyence Co., Osaka, Japan).

2.4 *In vitro* skin insertion

Miniature swine skin (Clawn strain, 1 month old) was purchased from Kagoshima Miniature Swine Research Center (Kagoshima, Japan). The hair on the skin samples was shaved and removed with a depilatory cream, and the fabricated MN array was applied on it using a spring-loaded applicator (5.3 m/s). The force for skin insertion by the applicator was approximately 17–19 N. Micropores on the

Journal : Large 10544 | Article No : 576 | Pages : 8 | MS Code : 576 | Dispatch : 20-7-2021

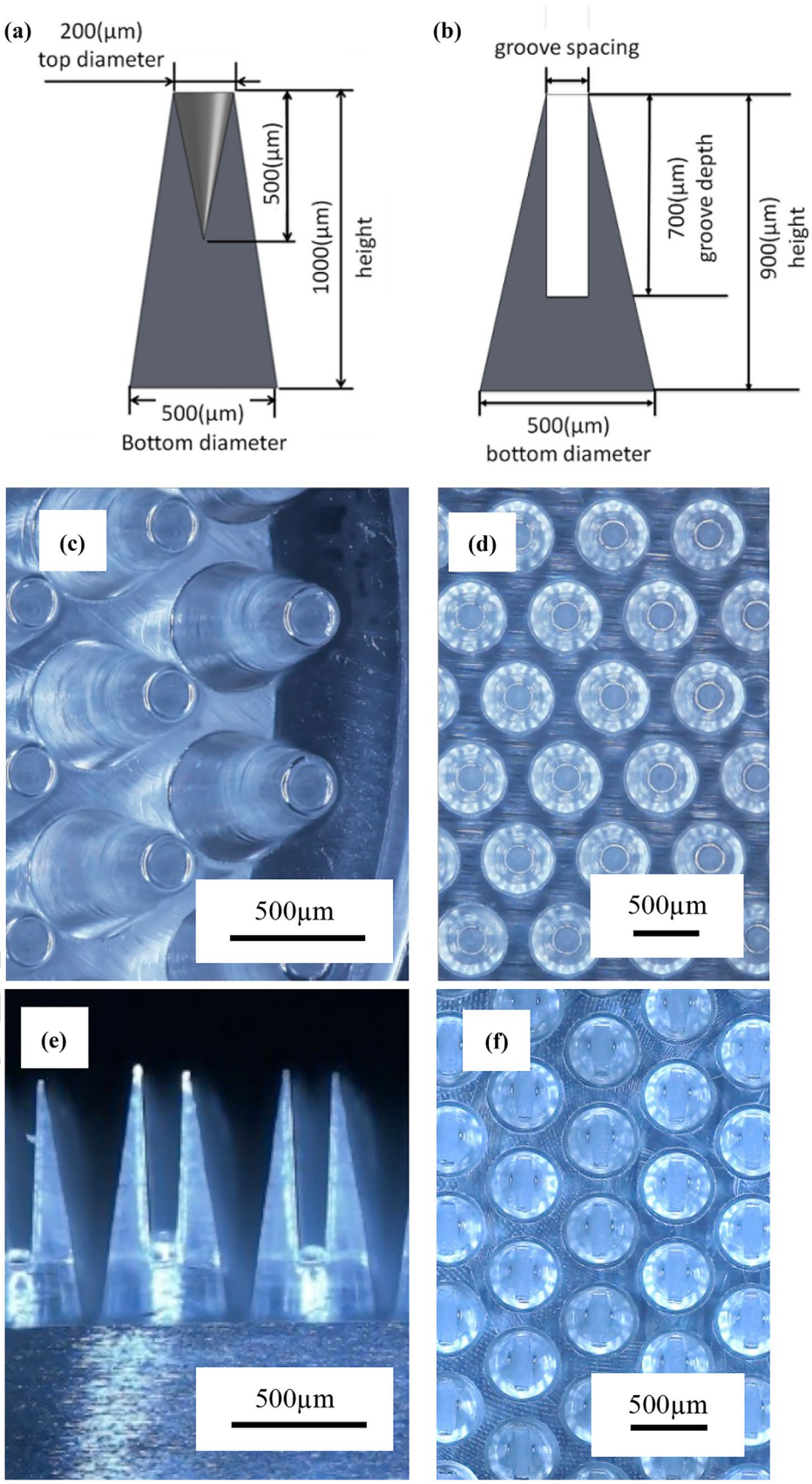

Fig. 1 Design of (**a**) a semi-hollow microneedle (MN) and (**b**) bird-bill MN. Photographs of semi-hollow MNs in (**c**) diagonal and (**d**) top view and bird-bill MNs in (**e**) side and (**f**) top view

Journal : **Large 10544**	Article No : **576**	Pages : **8**	MS Code : **576**	Dispatch : **20-7-2021**

skin were photographed using an optical coherent tomography (OCT) system (WP OCT 800-nm System, Wasatch Photonics Inc., Utah, USA). In addition, the depth of the micropores was determined using the OCT system (4 μm resolution of depth and transversal length).

2.5 Coating of the bird-bill MN

The bird-bill MN array was dipped in a coating gel made from Metolose® and a model drug, MB, or insulin. The coated MN was dried for 30 min at 20 °C and 50% humidity. Then, the weight of the coated MN was measured using an electronic scale. This process was repeated until the needle groove was filled with the drug gel, as indicated by no further increase in weight. Insulin-coated MN arrays (7.5% insulin and 20% Metolose®) were prepared the day before the *in vivo* animal experiments and were stored at 4 °C.

2.6 *In vivo* experiment

All animal experiments were conducted in accordance with our institutional guidelines and were approved by the Animal Care and Use Committee of the Kyushu Institute of Technology.

Rats (age, 8 weeks; weight, 266.7 ± 13.5 g; Jcl:SD strain, male; CLEA Japan Inc., Tokyo, Japan) were provided free access to food (CE-2, CLEA Japan Inc., Tokyo, Japan) and water for a week under standard conditions (temperature: 23 °C, humidity: 60%, 12:12 h light:dark cycle). Before the induction of diabetes, the rats were fasted for 16 h. Each was then administered an intraperitoneal injection of STZ (65 mg/kg dissolved in ice-cold 20 mM sodium citrate buffer, pH 4.6), and fed 3 h after the injection. Subsequently, the STZ-injected rats were provided free access to food and water for over a week, and rats with a fasting blood glucose concentration (BGC) greater than 250 mg/dL, polyuria, and polydipsia were considered diabetic.

The hair on the dorsal skin of diabetic rats was removed 48 h prior to skin piercing with the MN array using the applicator. After applying the semi-hollow MN, a cotton pad soaked with 1.0 mL insulin solution (200 IU) was loaded onto the pierced area. After 3 h, the treated area was wiped with a Kimwipe® (Nippon Paper Crecia, Co., Tokyo, Japan) and washed once with distilled water. The insulin-coated bird-bill MN was applied using the applicator and kept for 1 min on the skin. The rats were fasted but provided ad libitum access to water for all experiments. At predetermined time points, a drop of blood was collected from the tail vein, and the BGC was measured using a Medisafe® mini GR-102 (Terumo Co., Tokyo, Japan). Trans-epidermal water loss (TEWL) from the MN-treated skin was also measured using a Tewameter TM300 (Courage + Khazaka electronic GmbH, Köln, Germany). Rats treated with insulin solution (soaked into cotton) on intact skin and stripped skin (peeling of SC 20 times using adhesive tape) were used as negative control and positive control, respectively.

2.7 Statistical analysis

The arithmetic mean and standard deviation were calculated. A two-tailed Student's t-test was performed to compare the two different conditions. A p-value less than 0.05 was considered statistically significant.

3 Results and discussion

3.1 Fabrication of the semi-hollow MN arrays and the bird-bill MN arrays

A biodegradable polymer is better for the fabrication of MNs to reduce the risks associated with needle breakage (Lee et al. 2011). Because the mechanical aspect of MN is an important factor to estimate pain for insertion, we selected the biocompatible polymer PC. PC has a characteristic dimensional accuracy during molding, presents small changes in dimension after molding, and has high resistance to impact. Using a digital microscope, we demonstrated that the needles in the MN arrays did not bend or break after skin insertion.

Photographs of the semi-hollow MN array and the bird-bill MN array are shown in Fig. 1c–f, and the design values and actual measurements of the various parameters of the fabricated MNs are summarized in Table 1. The semi-hollow MN depth could not be measured because of the transparency of PC. The errors in the measured value (E_m) of the semi-hollow MNs with respect to the design values were 89.9% (height), 93.9% (top diameter), and 99.0% (bottom diameter). The height of the MN array did not reach the design value. This was caused by reduced gate pressure and consequent insufficient degassing of the mold. The dimensional variation coefficients (CVs) of the semi-hollow MNs were as follows: 1.59×10^{-2} (height), 1.63×10^{-2} (top diameter) and 1.73×10^{-2} (bottom diameter). Thus, the semi-hollow MNs had a uniform shape and quality. The E_m values of the bird-bill MNs were 97.2% (height), 98.3% (bottom diameter), 99.2% (groove depth), and 83.6% (groove spacing). The CVs were as follows: 2.98×10^{-2} (height), 2.04×10^{-2} (bottom diameter), 2.45×10^{-2} (groove depth), and 0.138 (groove spacing). The groove spacing of the MN array was narrow when compared with the design value, and it had a large CV value. The number of mold parts of the bird-bill MN was larger than that of the semi-hollow MN. Thus, the gap between the parts was present in the mold of the bird-bill MN. Although we tried to eliminate the

Journal : Large 10544 | Article No : 576 | Pages : 8 | MS Code : 576 | Dispatch : 20-7-2021

Table 1 Various parameters of the fabricated microneedle (MN) arrays

	Height (μm)	Bottom diameter (μm)	Top diameter (μm)	Groovr depth (μm)	Groove spacing (μm)
Design value	1,000	500	200	700	200
Semi-hollow MN	899.0 ± 14.3	494.8 ± 8.6	187.7 ± 3.1	——	——
Bird-bill MN	971.8 ± 29.0	491.4 ± 10.0	——	694.6 ± 17.0	167.2 ± 23.1

gap, there was still a gap in the groove of the bird-bill MN. The narrow distance between tips in the bird-bill MN was desirable to strengthen capillary attraction. We considered these results to indicate uniform quality in the arrays that were fabricated, and therefore, we used them in the following experiments.

3.2 Skin insertion capability of the fabricated MN arrays

To assess the skin insertion capability of the MN arrays, the depth of each micropore after insertion of the MN array *in vitro* was measured using the captured OCT images (Fig. 2). Micropores were maintained at 60 min after MN application (Fig. 2c, f). The depths of the puncture holes measured from the OCT images are shown in Fig. 2g. The puncture hole depths immediately after application of the semi-hollow MNs and the bird-bill MNs were 178.5 ± 27.6 μm and 232.1 ± 51.3 μm, respectively. These values were considered adequate to reach the capillary vessels of not only rats (Hikima et al. 2002) but also humans.

The time course of TEWL is shown in Fig. 3. The TEWL increased to 313 ± 132% immediately after application in the semi-hollow MN group, significantly differing from that of the control group ($p < 0.05$), and slowly decreased to baseline values over 3 h. The TEWL of the bird-bill MN group increased to 250.6 ± 77.7% after insertion and continued to maintain a high value of over 200% over 6 h. Zhou et al. (2010) reported the efficacy of transdermal insulin delivery in diabetic rats using commercially available solid MN rollers that pierced the skin and delivered insulin solution. It was observed that the TEWL increased two-fold after the application of MN rollers and recovered to control values within 3 h. In this study, measurements of puncture hole depth and TEWL showed that both MN arrays effectively opened the micro-holes on the SC and maintained them in that state for extended periods of time. These results indicated that both the fabricated MN arrays had sufficient skin-puncturing abilities.

3.3 Coating of the bird-bill MN arrays

Figure 4a shows the amount of coating gel (1% MB as a model drug and 10% Metolose®) applied during each coating cycle. The amount of the coating gel increased as the coating time increased, and it reached a maximum value of 3.20 ± 0.21 mg/MN array. Chen et al. (2017) reported that the maximum amount of drug coating one conical needle was 18 ng, and the total amount on the MN array (5 × 5) was estimated to be 450 ng. Baek et al. (2017) reported that the drug dose of the MN coated with 25% lidocaine was 290.6 ± 45.9 μg/MN array. Therefore, it was concluded that the amount of the coated drug on the bird-bill MN was sufficiently increased, when compared with other solid MNs. Figure 4b shows a microscopic image of the insulin-coated bird-bill MN. The average weight of the coating gel on the bird-bill MN was 1.17 ± 0.261 mg/MN array, and the gross weight of insulin was 93.2 ± 12.9 μg/MN array. This was assumed to be about 23.9 mIU/MN array, which can be considered as a sufficient amount of insulin for administration to diabetic rats (Chen et al. 2015; Lee et al. 2016).

3.4 Animal experiment

The BGC levels in diabetic rats subjected to SC piercing by the semi-hollow MN array were significantly decreased at all sampling time points, when compared with those of the negative controls ($p < 0.01$ or 0.05; ● in Fig. 5). After one application of the semi-hollow MN array, insulin was effective in controlling BGC within 30 min and the desired effect was maintained for 6 h. The sustained hypoglycemia may also be caused by the long-term micro-holes on the SC. Insulin is rapidly absorbed through the hole, and the spot with the highest insulin concentration was created in the epidermis under the hole. After removal of the cotton pad soaked with insulin and the skin surface was wiped using a Kimwipe®, we hypothesized that insulin from the spot slowly diffused throughout the epidermis and was absorbed into the microcirculation. In comparison, the BGC in rats subjected to piercing by solid MN decreased to less than 20% after 3 h, and returned to control values after the removal of the insulin solution (300 IU/mL) (Zhou et al. 2010). This result suggests the possibility of continuous insulin delivery to the skin because of the long-term micro-hole formation by the semi-hollow MN.

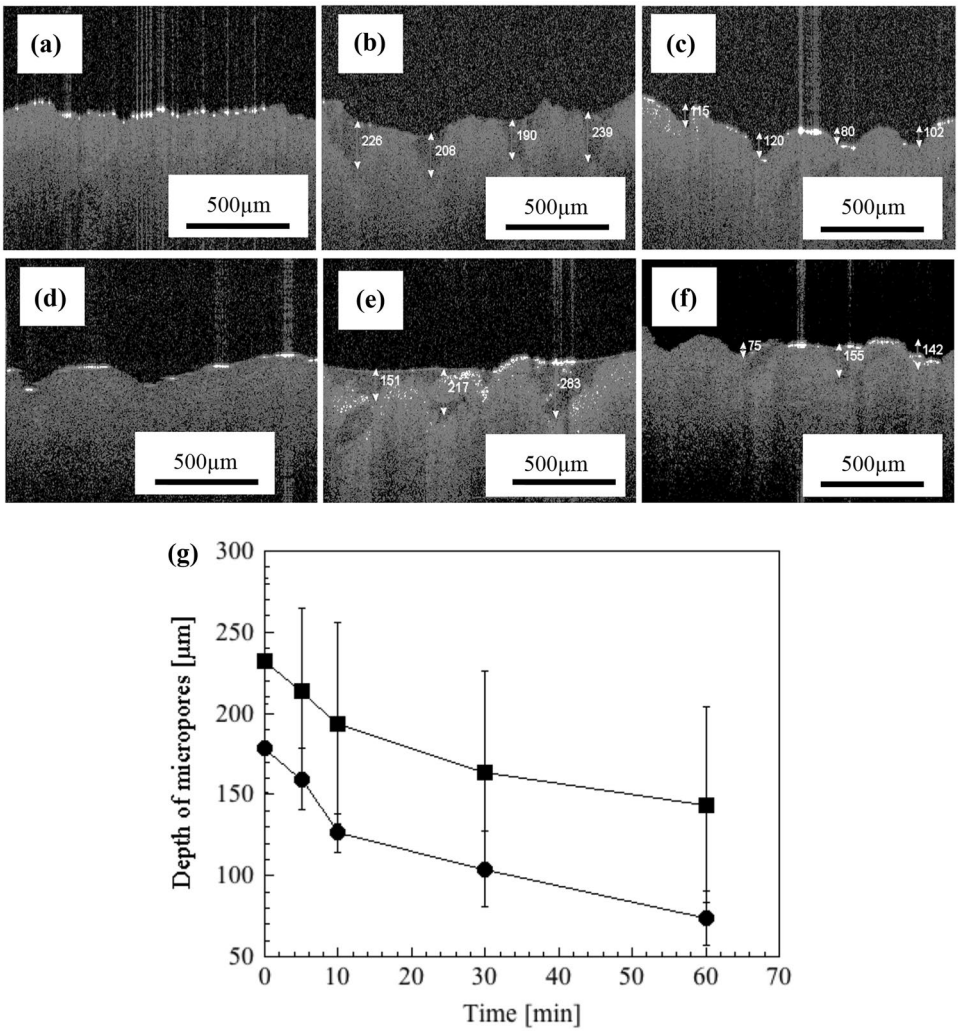

Fig. 2 Real-time optical coherent tomography imaging of micropores after the application of (**a–c**) semi-hollow microneedle (MN) and (**d–f**) bird-bill MN on rat skin and (**g**) time course of micropore depth treated with (●) semi-hollow MN and (■) bird-bill MN. Representative images of semi-hollow MN and bird-bill MN at each time (**a, d**) before insertion, (**b, e**) 0 min and (**c, f**) 60 min after insertion. The data points represent the mean ± S.D. of 4 experiments (**g**)

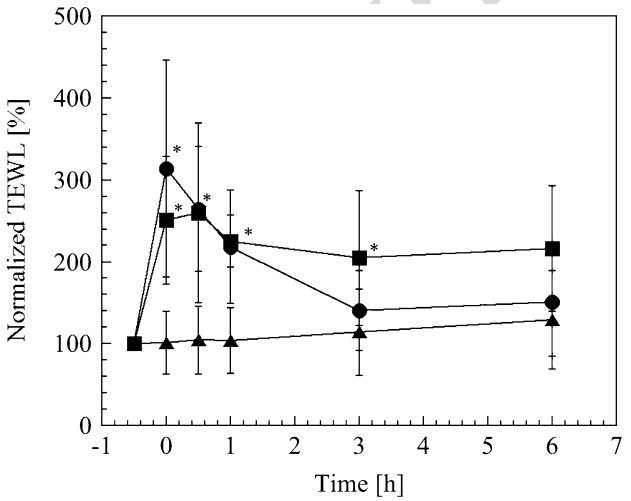

Fig. 3 Time course of trans-epidermal water loss (TEWL) treated with (●) semi-hollow microneedle (MN), (■) bird-bill MN and (▲) control (intact skin without MN treatment). The data points represent the mean ± S.D. of six experiments. *: $p < 0.05$ compared to control group at the same timepoint (Student's t-test)

The BGC decreased slowly 2 h after the application of the insulin-coated bird-bill MN (23.9 mIU) and reached a value of less than 60% BGC after 6 h (■ in Fig. 5). This was caused by only one shot and 1 min application of the bird-bill MN. This may be due to the residual coating gel containing insulin in the groove that slowly dissolved for a long-term in the micropore because the coating gel did not appear to fall off from the outside surface of the needle, which was verified using a microscope. A previous study by Zhang et al. (2018) reported that when a dissolving MN containing 5 IU insulin was applied to the skin surface for more than 5 min, the hypoglycemic effect lasted for 5 h. This suggests that the bird-bill MN, which had sufficient skin-puncturing ability, increased the amount of coated insulin in the vertical groove at the MN tip and could reduce the BGC within a minute of MN application.

Journal : Large 10544 | Article No : 576 | Pages : 8 | MS Code : 576 | Dispatch : 20-7-2021

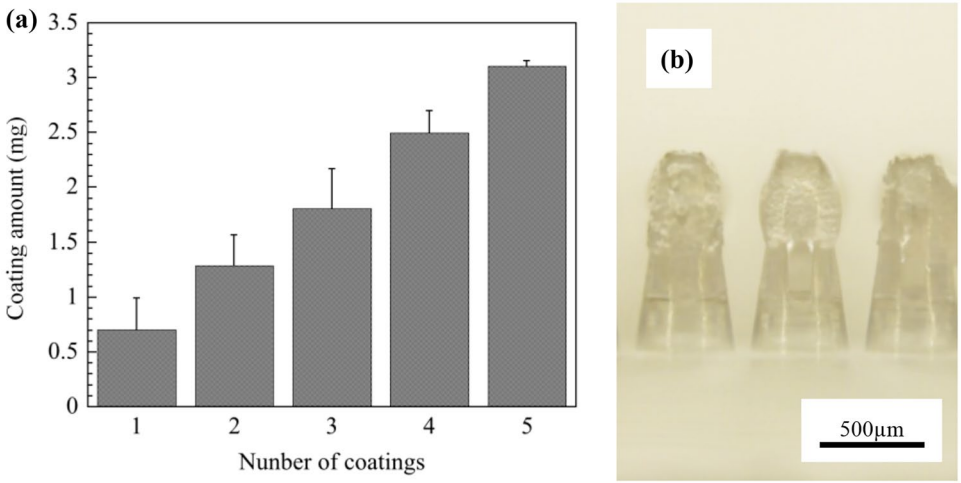

Fig. 4 Coating capacity on bird-bill microneedle (MN). (**a**) The amount of loaded gel on the bird-bill MN was measured during each coating cycle after dip coating (1% methylene blue trihydrate (MB) and 10% Metolose®). (**b**) Side-view photograph of the insulin-coated bird-bill MN

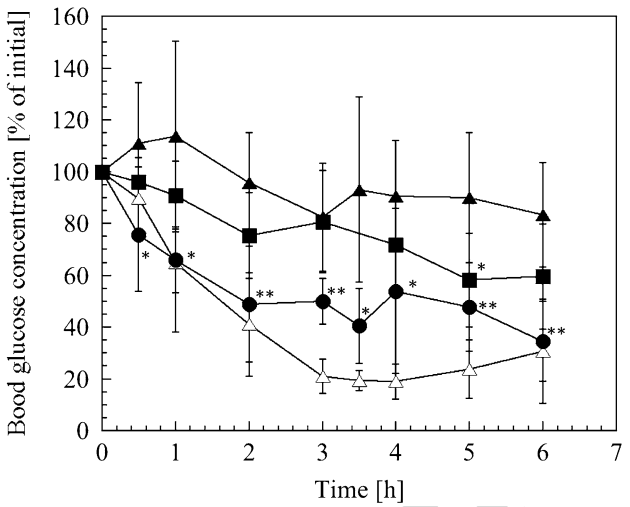

Fig. 5 Time course of blood glucose concentration in diabetic rats treated with (●) semi-hollow microneedle (MN), (■) bird-bill MN, (▲) negative control (insulin on the intact skin) and (△)positive control (insulin on the stripped skin). The data points represent the mean ± S.D. of more than 5 experiments. *: $p < 0.05$; **: $p < 0.01$, compared to the negative control at the same timepoint (Student's t-test)

4 Conclusions

We fabricated semi-hollow and bird-bill MN arrays with a mass-production capability and effective shapes for inducing micropore formation using the injection molding method. The semi-hollow MN arrays were suitable for maintaining micro-holes on the SC for an extended period. When the semi-hollow MNs were used for the transdermal delivery of insulin in diabetic rats, it was observed that the BGC decreased significantly within 30 min, and the desired effect of insulin was maintained for an additional 3 h after the removal of insulin from the skin surface. Moreover, the bird-bill MN was able to load a coating gel at a maximum capacity of 3.20 ± 0.21 mg per MN array, and the BGC continued to decrease significantly for 2–6 h. The two MN arrays could provide effective transdermal delivery of the large-molecular-weight drug, namely insulin. Some problems may be solved by modification of the mold. The shape, number, diameter and angle of the MN, as well as the groove spacing, can be optimized to maximize the coating dose and for deeper insertion into the skin. Further studies are required to evaluate whether the developed MNs can be used for the delivery of other large-molecular- weight drugs consisting of nucleic acids and proteins.

Acknowledgements This work was supported by the Japan Society for the Promotion of Science (JSPS) KAKENHI Grant Number JP.18K12109.

References

S.-H. Baek, J.-H. Shin, Y.-C. Kim, Drug-coated microneedles for rapid and painless local anesthesia. Biomed. Microdevices **19**, 2 (2017). https://doi.org/10.1007/s10544-016-0144-1

M.-C. Chen, M.-H. Ling, S.J. Kusuma, Poly-γ-glutamic acid microneedles with a supporting structure design as a potential tool for transdermal delivery of insulin. Acta Biomater. **24**, 106–116 (2015). https://doi.org/10.1016/j.actbio.2015.06.021

Y. Chen, B.Z. Chen, Q.L. Wang, X. Jin, X.D. Guo, Fabrication of coated polymer microneedles for transdermal drug delivery. J. Control Release **265**, 14–21 (2017). https://doi.org/10.1016/j.jconrel.2017.03.383

K. Cheung, T. Han, D.B. Das, Effect of Force of Microneedle Insertion on the Permeability of Insulin in Skin. J. Diabetes Sci. Technol. **8**, 444–452 (2014). https://doi.org/10.1177/1932296813519720

S.N. Economidou, C.P.P. Pere, A. Reid, J. Uddim, J.F.C. Windmill, D.A. Lamprou, D. Douroumis, 3D printed microneedle patches using stereolithography (SLA) for intradermal insulin delivery.

Mater. Sci. Eng. C **102**, 743–755 (2019). https://doi.org/10.1016/j.msec.2019.04.063

H.S. Gill, M.R. Prausnitz, Pocketed microneedles for drug delivery to the skin. J. Phys. Chem. Solids **69**, 1537–1541 (2008). https://doi.org/10.1016/j.jpcs.2007.10.059

M. Han, D.K. Kim, S.H. Kang, H.-R. Yoon, B.-Y. Kim, S.S. Lee, K.D. Kim, H.G. Lee, Improvement in antigen-delivery using fabrication of a grooves-embedded microneedle array. Sens. Actuators B Chem. **137**, 274–280 (2009). https://doi.org/10.1016/j.snb.2008.11.017

T. Hikima, K. Yamada, T. Kimura, H.I. Maibach, K. Tojo, Comparison of skin distribution of hydrolytic activity for bioconversion of β-estradiol 17-acetate between man and several animals *in vitro*. Eur. J. Pharm. Biopharm. **54**, 155–160 (2002). https://doi.org/10.1016/s0939-6411(02)00084-x

X. Jin, D.D. Zhu, B.Z. Chen, M. Ashfaq, X.D. Guo, Insulin delivery systems combined with microneedle technology. Adv. Drug Deliv. Rev. **127**, 119–137 (2018). https://doi.org/10.1016/j.addr.2018.03.011

A.R. Johnson, C.L. Caudill, J.R. Tumbleston, C.J. Bloomquist, K.A. Moga, A. Ermoshkin, D. Shirvanyants, S.J. Mecham, J.C. Luft, J.M. DeSimone, Single-Step Fabrication of Computationally Designed Microneedles by Continuous Liquid Interface Production. PLoS One **11**(2016)

M.J. Kim, S.C. Park, B. Rizal, G. Guanes, S.-K. Baek, J.-H. Park, A.R. Betz, S.-O. Choi, Fabrication of Circular Obelisk-Type Multilayer Microneedles Using Micro-Milling and Spray Deposition. Front. Bioeng. Biotechnol. **6**, 54 (2018). https://doi.org/10.3389/fbioe.2018.00054

S.F. Lahiji, Y. Kim, G. Kang, S. Kim, S. Lee, H. Jung, Tissue Interlocking Dissolving Microneedles for Accurate and Efficient Transdermal Delivery of Biomolecules. Sci. Rep. **9**, 7886 (2019). https://doi.org/10.1038/s41598-019-44418-6

E. Larrañeta, R.E.M. Lutton, A.D. Woolfson, R.F. Donnelly, Microneedle arrays as transdermal and intradermal drug delivery systems: Materials science, manufacture and commercial development. Mater. Sci. Eng. R **104**, 1–32 (2016). https://doi.org/10.1016/j.mser.2016.03.001

I.-C. Lee, W.-M. Lin, J.-C. Shu, S.-W. Tsai, C.-H. Chen, M.-T. Tsai, Formulation of two-layer dissolving polymeric microneedle patches for insulin transdermal delivery in diabetic mice. J. Biomed. Mater. Res. A **105**, 84–93 (2016). https://doi.org/10.1002/jbm.a.35869

K. Lee, C.Y. Lee, H. Jung, Dissolving microneedles for transdermal drug administration prepared by stepwise controlled drawing of maltose. Biomaterials **32**, 3134–3140 (2011). https://doi.org/10.1016/j.biomaterials.2011.01.014

C. Plamadeala, S.R. Gosain, F. Hischen, B. Buchroithner, S. Puthukodan, J. Jacak, A. Bocchino, D. Whelan, C. O'Mahony, W. Baumgartner, J. Heitz, Bio-inspired microneedle design for efficient drug/vaccine coating. Biomed. Microdevices **22**, 8 (2020). https://doi.org/10.1007/s10544-019-0456-z

F. Ribet, G. Stemme, N. Roxhed, Real-time intradermal continuous glucose monitoring using a minimally invasive microneedle-based system. Biomed. Microdevices **20**, 101 (2018). https://doi.org/10.1007/s10544-018-0349-6

A.M. Römgens, D.L. Bader, J.A. Bouwstra, F.P. Baaijens, C.W.J. Oomens, Monitoring the penetration process of single microneedles with varying tip diameters. J. Mech. Behav. Biomed Mater. **40**, 397–405 (2014). https://doi.org/10.1016/j.jmbbm.2014.09.015

F. Ruggiero, R. Vecchione, S. Bhowmick, G. Coppola, S. Coppola, E. Esposito, V. Lettera, P. Ferraro, P.A. Netti, Electro-drawn polymer microneedle arrays with controlled shape and dimension. Sens. Actuators B. Chem. **255**, 1553–1560 (2018). https://doi.org/10.1016/j.snb.2017.08.165

Y. Zhang, G. Jiang, W. Yu, D. Liu, B. Xu, Microneedles fabricated from alginate and maltose for transdermal delivery of insulin on diabetic rats. Mater. Sci. Eng. C **85**, 18–26 (2018). https://doi.org/10.1016/j.msec.2017.12.006

C.-P. Zhou, Y.-L. Liu, H.-L. Wang, P.-X. Zhang, J.-L. Zhang, Transdermal delivery of insulin using microneedle rollers *in vivo*. Int. J. Pharm. **392**, 127–133 (2010). https://doi.org/10.1016/j.ijpharm.2010.03.041